MANAGING AN SIR EPIDEMIC SYSTEM VIA OPTIMAL CONTROL OF TRANSMISSION RATE

Anonymous authors
Paper under double-blind review

ABSTRACT

Shaping an epidemic with adaptive contact restriction policies has been the holy grail during the COVID-19 pandemic. In this paper, we explore the problem of determining the optimal control policy for transmission rate assuming SIR dynamics. We first demonstrate that the SIR model with infectious patients and susceptible contacts (i.e., product of transmission rate and susceptible population) interpreted as predators and prey respectively maps to a Lotka-Volterra (LV) predator-prey model. The modified SIR system (LVSIR) has a stable equilibrium point, an "energy" conservation property, and exhibits bounded cyclic behaviour similar to an LV system. We exploit this mapping using a control-Lyapunov approach to design a novel, practical control policy (CoSIR) that nudges the SIR model to the desired equilibrium. Empirical comparison with periodic lockdowns on simulated and real COVID-19 data demonstrates the efficacy and adaptability of our approach.

1 INTRODUCTION

The COVID-19 situation and its immense toll on human lives has highlighted the enormous public health challenges associated with managing a pandemic. Contact restrictions via lockdowns and social distancing have emerged as a powerful policy instrument, especially in low and middle income countries, which cannot afford to scale up testing, medical capacity, and vaccinations. However, choosing the optimal level of restrictions is highly non-trivial because of the complex trade-off between the disease and socioeconomic impacts, and the evolving situation on the ground.

Public health interventions related to COVID-19 have largely been driven by scenario-based epidemiological forecasting (Ferguson et al., 2020) with decision-making based on comparison of a few restricted scenarios. Though valuable, this approach lean towards a reactive role for the health authorities. In contrast, less attention has been devoted to developing an analytic control framework to support proactive decision-making based on the target disease and economic outcomes, and the state of the epidemic. Multiple studies (Chowdhury et al., 2020; Killian et al., 2020; Bin et al., 2020) point to the benefits of periodic lockdowns, but these interventions are based on simulations of limited scenarios and are not adaptive in nature. Some recent works (Acemoglu et al., 2020) formulate the control problem in terms of the net socioeconomic and disease impact but require an expensive numerical solution. Recent reinforcement learning approaches (Bhardwaj et al., 2020) are efforts in similar direction but do not fully exploit the mathematical structure of the epidemic dynamics.

Problem formulation. During an epidemic, a key concern for public health officials is to determine the right level and schedule of contact restrictions that balances the disease and socioeconomic burdens. For tractability, we assume that the public health goal is to limit infections to a certain target level determined via an independent impact analysis (BMGF, 2020). The problem can then be framed in terms of determining an adaptive policy that achieves this target.

For a given region, let (N, S_{curr}, I_{curr}) be the total, current susceptible, and infectious populations respectively. Let (I_{avg}^{target}, I_{max}^{target}) be the target average and maximum infectious levels. Let $\mathcal{A}$ be the set of social-restriction levels for which the transmission rate can be estimated (COVID-AMP (2020), Table 4) and T, the decision horizon, then the goal is to identify restriction levels $[a_t]$, $[t]_{curr+1}^{curr+T}$, $a_t \in \mathcal{A}$ such that the infectious level averages at I_{avg}^{target} but does not exceed I_{max}^{target}.

Contributions. We establish a novel mapping between SIR dynamics and the Lotka-Volterra (LV) system (Baigent, 2016) by interpreting infectious patients as predators and susceptible contacts as the prey, under a specific transmission rate policy. The resulting system (`LVSIR`) has a stable

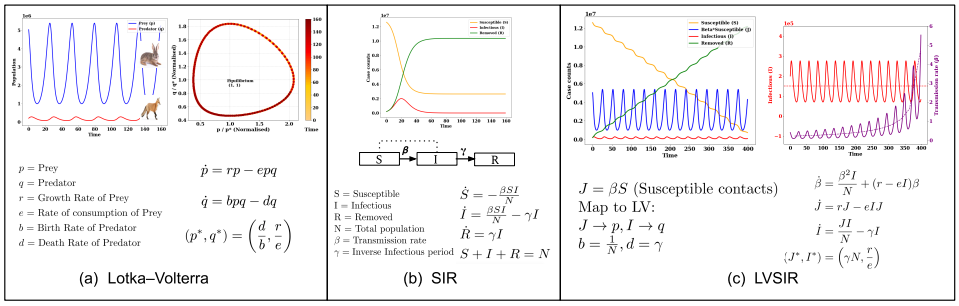

Figure 1: (a) LV system and time evolution of predator and prey populations, (b) SIR compartmental dynamics, (c) SIR model to LV system mapping and the behaviour of case counts S, J, I, R and transmission rate β.

equilibrium point and an "LV energy" conservation property. We derive an optimal control policy for transmission rate (CoSIR) using control-Lyapunov functions (Tsinias, 1988) based on the "LV energy". This policy converges to the desired equilibrium (target infectious level) from any valid initial state. We also propose a practical approximate implementation (`CoSIR-approx`) assuming discrete levels and statistical estimation of other model parameters. Simulation results on real and synthetic COVID-19 data demonstrate the efficacy and adaptability of our approach.

2 Transmission Rate Control

Solving the restriction policy optimization is our primary goal. To achieve this, we first establish a connection between the SIR model and LV system, which is more amenable to control Meza et al. (2005) and then leverage the LV system properties to propose a strategy for transmission control.

SIR Compartmental Model. The SIR model is the simplest and most widely used epidemiological model comprising three compartments: Susceptible (**S**), Infectious (**I**) and Removed (**R**) with the dynamics shown in Figure 1(b). Here, β is the rate of disease transmission and γ is the inverse of the average infectious period.

Lotka-Volterra (LV) Systems. LV systems model the population dynamics of predator-prey species in an ecosystem (see Figure 1(a)). The growth rate of prey population p depends on its reproduction rate r and the rate of consumption by predator e. The change in predator population q depends on the nourishment-based birth rate b and its death rate d. The system has two fixed points: (a) a saddle point that maps to extinction $(p, q) = (0, 0)$, and (b) a stable equilibrium at $(p, q) = (\frac{d}{b}, \frac{r}{e})$. Typically, the system exhibits oscillations resulting in a closed phase plot that corresponds to conservation of a "LV energy" function.

SIR-LV Mapping. Stabilizing infection levels has a direct analogy with population control in predator-prey systems where it is desirable to maintain the predator and prey population at certain target levels suitable for the ecosystem. Comparing the SIR and LV dynamics in Figure 1, we observe that the behaviour of the infectious population (I) is similar to that of the "predators" (q). There is an inflow (birth) $\beta SI/N$ and an outflow (death) γI. An intuitive choice for "prey" is the "susceptible contacts" (i.e., the product of susceptible people and β, the average per-day contacts) since this acts as "nourishment" to the predators and contributes to the inflow into the **I** compartment. Denoting the susceptible contacts by $J \coloneqq \beta S$, we note that equivalence with the LV system requires $\dot{J} = \dot{\beta}S + \dot{S}\beta = (r - eI)J = (r - eI)\beta S$, where r and e correspond to the reproduction rate and consumption rate of an LV system as described above. Since $\dot{S} = -\beta IS/N$, we require the transmission rate β to follow $\dot{\beta} = (r - eI)\beta + \beta^2 I/N$ [**LVSIR**].

This modification of SIR model (LVSIR) maps to a Lotka-Volterra system. The inverse of the infectious period (γ) corresponds to the predator death rate (d) and the inverse of population $(1/N)$ to the predator birth rate (b). The LV reproductive rate (r) and prey consumption rate (e) are extra degrees of freedom. Theorem 1 asserts the existence of a steady state for an epidemic following LVSIR dynamics and characterizes the oscillatory behavior and the energy conservation property.

Theorem 1 [1] *For the LVSIR model in Figure 1(c), the following properties hold true:*
(a) There exists a stable equilibrium for the system at $(J^*, I^*) = (\gamma N, r/e)$.
(b) When the initial state $(J_0, I_0) = (J^*, I^*)$*, then* (J, I) *is constant while* S, R *take a linear form.*

Algorithm 1 Practical Transmission Rate Control

Input:
N – Population,
$\mathcal{A}$ – Restriction policy levels,
$\rho : \mathcal{A} \mapsto \mathbb{R}_{++}$ – Map of levels to transmission rate,
$[S_t, I_t, R_t, a_t], [t]_0^{curr}$ – Case counts & restriction history,
$I_{max}^{target}, I_{avg}^{target}$ – max and avg., target infection levels,
T – Decision horizon,
T_{period} – Cyclic period for restriction schedule
Output:
$\mathbf{a}^* = [a_t],\ [t]_{curr+1}^{curr+T},\ a_t \in \mathcal{A}$ – Near optimal restriction levels for next T time units s.t. infection levels conform to I_{avg}^{target} and I_{max}^{target}.
Method:
Data-driven Calibration:
$\gamma \leftarrow \text{COMPUTEGAMMA}([S_t, I_t, R_t],\ [t]_0^{curr}, N)$
$\rho \leftarrow \text{REFINEBETAMAP}([S_t, I_t, R_t, a_t],\ [t]_0^{curr}, N)$
Choosing CoSIR Parameters:
$\hat{\beta}_{curr} \leftarrow \frac{\gamma N}{S_{curr}}$
$(J^*, I^*) \leftarrow (\gamma N, I_{avg}^{target})$
$\alpha \leftarrow (y - \log(y) - 1)$ where $y = \frac{I_{max}^{target}}{I_{avg}^{target}}$
$r \leftarrow \frac{(2\pi)^2}{\gamma T_{period}^2}$ for $\alpha \simeq 0$
(or chosen s.t. $g(r, \gamma, \alpha) = T_{period}$ for $\alpha >> 0$ where $g(\cdot)$ is as defined in Theorem 1.)
$e \leftarrow \frac{r}{I^*}$
$\eta \leftarrow$ DESIRED CONVERGENCE RATE
Determine Optimal Restrictions:
$[\beta_t^{ideal}], [t]_{curr+1}^{curr+T} \leftarrow$
$\text{CoSIR}(N, S_{curr}, I_{curr}, R_{curr}, \hat{\beta}_{curr}, r, e, \gamma, \eta, T)$
$a_t = \text{ARGMIN}_{a \in \mathcal{A}} (\beta_t^{ideal} - \rho(a))^2,\ [t]_{curr+1}^{curr+T}$
return $\mathbf{a}^* = [a_t],\ [t]_{curr+1}^{curr+T}$

Algorithm	Description
`No-Restrictions`	Constant $\beta = 0.44$.
`PL-high`	Periodic Lockdown of 60 days with $\beta = 0.16$ and a relaxation period of 30 days with $\beta = 0.44$.
`PL-low`	Periodic Lockdown of 60 days with $\beta = 0.1$ and a relaxation period of 30 days with $\beta = 0.44$.
`CoSIR`	Follows Eqn. 4.
`CoSIR-approx`	Approximation of CoSIR. β with 10 levels starting from 0.1 to 0.55 in steps of 0.05.

Table 1: Transmission control policies used for simulation.

Factor	Symbol	Hypothetical	India
Population	N	13M	1.36B
Susceptible Population	S_{curr}	12.6M	1.36B
Infectious Population	I_{curr}	0.2M	279k
Hospitalization ratio	h	-	2%
Target manageable I	I_{avg}^{target}	0.15M	6.8M
Target max to avg ratio	$\frac{I_{max}^{target}}{I_{avg}^{target}}$	1.3	1.13
Target H inflow	ΔH_{avg}^{target}	-	27.5k
Periodicity	T_{period}	7 days	7 days
Inverse Infectious period	γ	0.2	0.2
LV Reproduction rate	r	4.2	4.2
Consumption rate	e	r/I^*	r/I^*
Learning rate	η	5	5

Table 2: CoSIR parameters used in Section 3.

When $(J_0, I_0) \neq (J^*, I^*)$ it exhibits a cyclic behaviour with the following properties:
(c) The system "energy" $w(J, I) = \gamma(x - \log(x) - 1) + r(y - \log(y) - 1)$ (where $x = \frac{J}{J^*}, y = \frac{I}{I^*}$) remains constant at $w_0 = w(J_0, I_0) \geq w(J^*, I^*) = w^* = 0$ till termination.
(d) The I, J curves exhibit periodic oscillations resulting in a closed trajectory. The normalized phase plot has four extreme points $\{(x_{min}, 1), (1, y_{min}), (x_{max}, 1), (1, y_{max})\}$ where $(x_{min},\ x_{max})$ are the roots of the equation $x - \log(x) = 1 + w_0/\gamma$ and (y_{min}, y_{max}) are the roots of the equation $y - \log(y) = 1 + w_0/r$.
(e) The cyclic period T_{period} has the form $g(r, \gamma, \frac{w_0}{r})$ for a well-defined function $g(\cdot)$ (see Theorem A.2) with approximation via linearization yielding $T_{period} \simeq 2\pi/\sqrt{(r\gamma)}$.
(f) In each cyclic period, the susceptible population S reduces by a fixed amount $\Delta S = \gamma I^* T_{period}$. When $S < \Delta S$ at the start of a cycle, the epidemic terminates during that cycle.

Figure 1(c) depicts the oscillatory behaviour of the LVSIR model for the configuration in Table 2. Similar to an LV system, the "energy" which corresponds to a weighted Itakura-Saito distance between (I, J) and the equilibrium (I^*, J^*) is conserved. The infectious population I (and susceptible contacts J) oscillates between the extreme points with an average value of I^* (and J^*) while the susceptible population reduces steadily in a staircase-like fashion. The transmission rate β also exhibits oscillations but the average steadily goes up to compensate for the reduction in the susceptible population. Figures 2(b) shows the typical phase plot while Figure 2(a) depicts the behavior when initial state is itself the equilibrium.

Design of Optimal Control. Consider an epidemic system from a control theory perspective with the infectious population as the output. The SIR dynamics has a positive feedback loop leading to early exponential-like behavior. While the LVSIR dynamics neutralizes this feedback loop to exhibit oscillatory behavior, it does not converge to an equilibrium. Optimal control of such non-linear dynamical systems (i.e., nudging infectious levels to a desired equilibrium in our context) relies on the existence of control-Lyapunov functions (CLFs) typically derived from the associated conservation laws. We follow a similar approach to construct CLFs from the "Lotka-Volterra energy" function $w(J, I)$. Once a suitable Lyapunov function is identified, there exist multiple control strategies such as feedback linearization that are guaranteed to converge using Artstein's theorem (Artstein, 1983).

Let $L(w) : \mathbb{R}_+ \mapsto \mathbb{R}$ be a continuously differentiable function s.t. $|dL/dw| > 0$ and $L(w) > 0,\ \forall w$ and $L(w) = 0 \iff w = 0$. It can be shown that (Theorem B.1) $L(w(J, I))$ is a CLF for the SIR model and a proportional additive control of the form $\dot{\beta} = (r - eI)\beta + \beta^2 I/N + u\beta$ converges to the equilibrium (J^*, I^*) when $u = -\eta(t)\frac{dL}{dw}(\frac{J}{J^*} - 1)$ with the learning rate $\eta(t) > 0,\ \forall t$ **[CoSIR]**.

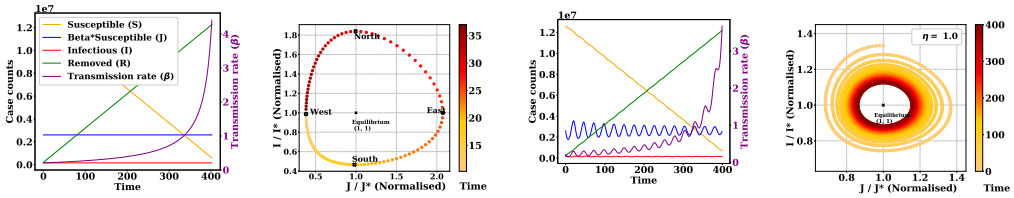

(a) (b) (c) (d)

Figure 2: (a) System (S, J, I, R, β) evolution when initialized at equilibrium. (b) Phase plot of the LVSIR model annotated with extreme points. (c-d) System evolution of the CoSIR model for learning rate $\eta = 1$.

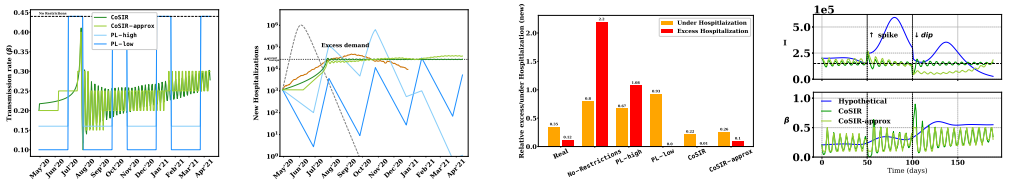

(a) (b) (c) (d)

Figure 3: Plots (a-c) show the $\beta(t)$, hospitalization inflow, and its comparison to ΔH_{avg}^{target} for various policies in India. (d) Shows the adaption of CoSIR variants in case of sudden increase or decrease ($t = 50, 100$).

Figures 2(c) show the damping oscillatory behavior of the CoSIR model for the case where $L(w) = w^2/2$. The β-control policy can be interpreted as follows. The first term $\beta^2 I/N$ corresponds to the relaxation due to the decreasing susceptibility while the second term $(r - eI)\beta$ leads to oscillatory behavior, and the last term $u\beta$ ensures dissipation of energy and convergence to the equilibrium. Even with external perturbations, the system can recalibrate β as appropriate.

Algorithm 1 outlines a practical approach that combines the optimal β-control (CoSIR) with estimation of parameters from historical data (ComputeGamma,RefineBetaMap) using traditional SIR calibration algorithms (Bettencourt & Ribeiro, 2008; Chu et al., 2011). Public health requirements such as infection level targets and periodicity are mapped to CoSIR parameters using Theorem 1. Optimal β is approximated by the "closest" (in squared loss) discrete level (`CoSIR-approx`).

3 Empirical Results

Experimental Setup. We compared two CoSIR variants with three baseline policies (Chowdhury et al., 2020) for transmission control and the real outcome (till 29th Dec 2020) for the COVID-19 pandemic in India (Table 1). Table 2 enumerates the relevant parameters (discussed in detail in Appendix C). We choose the target infectious level in terms of manageable hospital inflow ΔH_{avg}^{target} noting that hospitalizations in SIR model are given by $\gamma I h$ so that $I_{avg}^{target} = \Delta H_{avg}^{target} (\gamma h)^{-1}$.

Hospital Influx. Figure 3(a) shows the simulated daily new hospitalizations ($\gamma h I$). Real hospitalizations are obtained by appropriate scaling of the reported active cases accounting for under reporting (see Appendix C) and indicate periods where the healthcare system was overwhelmed. Figure 3(c) depicts the average excess and under hospital inflow relative to the target rate. `CoSIR` variants result in smaller deviations from the target levels. The key takeaway is that optimizing utilization requires choosing β based on the available medical capacity and the varying susceptibility.

Adaptability of CoSIR. Figure 3 shows the epidemic evolution of the two CoSIR variants along with a `hypothetical` but a realistic premature relaxation policy. The CoSIR variants not only stabilize infections, but are able to adapt to sudden upward ($t = 50$) or downward perturbations ($t = 100$) and continue pushing towards the equilibrium.

4 Conclusion & Future Work

We propose an analytical framework for epidemic control to support an active goal-oriented public health response. This framework relies on a mapping between SIR dynamics to LV systems under a specific transmission rate policy (LVSIR) and an additional feedback control mechanism (CoSIR). Given the vast literature on control of LV systems, this mapping can be leveraged to design new epidemic control techniques as well as extend current results to richer models and additional control variables. Results in diverse settings point to the potential utility of this approach. Practical deployment requires addressing lags in communication systems and incorporation of additional signals.

REFERENCES

Daron Acemoglu, Victor Chernozhukov, Iván Werning, and Michael D Whinston. Optimal targeted lockdowns in a multi-group SIR model. *NBER Working Paper*, 27102, 2020.

Zvi Artstein. Stabilization with relaxed controls. *Nonlinear Analysis: Theory, Methods & Applications*, 7(11):1163–1173, 1983. doi: 10.1016/0362-546X(83)90049-4.

Stephen Baigent. Lotka-Volterra dynamics: An introduction. 2016.

Luís M. A. Bettencourt and Ruy M. Ribeiro. Real time Bayesian estimation of the epidemic potential of emerging infectious diseases. *PLOS ONE*, 3(5):1–9, 2008.

Ankit Bhardwaj, Han Ching Ou, Haipeng Chen, Shahin Jabbari, et al. Robust lock-down optimization for COVID-19 policy guidance. In *AAAI Fall Symposium*, 2020.

Michelangelo Bin, Peter Cheung, Emanuele Crisostomi, Pietro Ferraro, et al. On fast multi-shot COVID-19 interventions for post lock-down mitigation, 2020.

BMGF. COVID-19: A Global Perspective, 2020. URL `https://www.gatesfoundation.org/goalkeepers/report/2020-report/#GlobalPerspective`.

W.E. Boyce, R.C. DiPrima, and D.B. Meade. *Elementary Differential Equations and Boundary Value Problems*. Wiley, 2017. ISBN 9781119443766.

Rajiv Chowdhury, Kevin Heng, Md Shajedur Rahman Shawon, et al. Dynamic interventions to control COVID-19 pandemic: a multivariate prediction modelling study comparing 16 worldwide countries. *European Journal of Epidemiology*, 35(5):389–399, 2020. doi: 10.1007/s10654-020-00649-w.

Wei Chu, Lihong Li, Lev Reyzin, and Robert Schapire. Contextual bandits with linear payoff functions. In *Proceedings of the Fourteenth International Conference on Artificial Intelligence and Statistics*, volume 15 of *Proceedings of Machine Learning Research*, pp. 208–214, Fort Lauderdale, FL, USA, 11–13 Apr 2011.

COVID-AMP. Analysis and mapping of policies - COVID-AMP, 2020. URL `https://covidamp.org/`.

COVID19India. Coronavirus in India: Latest Map and Case Count, 2020. URL `https://www.covid19india.org/`.

Neil Ferguson, Daniel Laydon, Gilani G Nedjati, N Imai, K Ainslie, et al. Report 9: Impact of non-pharmaceutical interventions (NPIs) to reduce COVID19 mortality and healthcare demand. Technical report, Imperial College, London, 2020.

Sze-Bi Hsu. A remark on the period of the periodic solution in the Lotka-Volterra system. *Journal of Mathematical Analysis and Applications*, 95(2):428–436, 1983. doi: 10.1016/0022-247X(83)90117-8.

Jackson A. Killian, Marie Charpignon, Bryan Wilder, Andrew Perrault, et al. Evaluating COVID-19 lockdown and business-sector-specific reopening policies for three US states. In *KDD 2020 Workshop on Humanitarian Mapping*, 2020. doi: 10.2139/ssrn.3598744.

Gideon Meyerowitz-Katz and Lea Merone. A systematic review and meta-analysis of published research data on COVID-19 infection-fatality rates. *medRxiv*, 2020.

Magno Enrique Mendoza Meza, Amit Bhaya, and Eugenius Kaszkurewicz. Controller design techniques for the Lotka-Volterra nonlinear system. *SBA: Controle & Automaccão Sociedade Brasileira de Automatica*, 16:124 – 135, 2005. ISSN 0103-1759. doi: 10.1590/S0103-17592005000200002.

Siuli Mukhopadhyay and Debraj Chakraborty. Estimation of undetected COVID-19 infections in India. *medRxiv*, 2020. doi: 10.1101/2020.04.20.20072892.

Manoj V Murhekar, Tarun Bhatnagar, Sriram Selvaraju, Kiran Rade, et al. Prevalence of SARS-CoV-2 infection in India: Findings from the national serosurvey, May-June 2020. *Indian Journal of Medical Research*, 152(1):48, 2020.

OECD. Hospital beds, Dec 2020. URL `https://data.oecd.org/healtheqt/hospital-beds.htm`.

P Joseph Phillip, Ross Mullner, and Steven Andes. Toward a better understanding of hospital occupancy rates. *Health Care Financing Review*, 5(4):53, 1984.

Yuri Aleksandrovich Pykh. Lyapunov functions for Lotka-Volterra systems: An overview and problems. *IFAC Proceedings Volumes*, 34(6):1549 – 1554, 2001. ISSN 1474-6670. doi: 10.1016/S1474-6670(17)35410-1.

Shagi-Di Shih. The period of a Lotka-Volterra system. *Taiwanese Journal of Mathematics*, 1(4): 451–470, 1997. ISSN 10275487, 22246851.

John Tsinias. Stabilization of affine in control nonlinear systems. *Nonlinear Analysis: Theory, Methods & Applications*, 12(11):1283 – 1296, 1988. ISSN 0362-546X. doi: 10.1016/0362-546X(88)90060-0.

John Tsinias. Sufficient Lyapunov-like conditions for stabilization. *Mathematics of Control, Signals and Systems*, 2(4):343–357, 1989. ISSN 1435-568X. doi: 10.1007/BF02551276.

A LVSIR System Properties

Definition A.1 *(Boyce et al., 2017) Let $\mathbf{z}^* \in \mathbb{R}^n$ be a critical point of a system of ODEs. The critical point $\mathbf{z}^*$ is stable if, for any $\epsilon > 0$ $\exists\ \delta > 0$ such that if $\mathbf{z} = \phi(t)$ satisfies $||\phi(0) - \mathbf{z}^*|| < \delta$ then $||\phi(t) - \mathbf{z}^*|| < \epsilon,\ \forall\ t > 0$.*

Theorem A.1 [1] *For the LVSIR model in Figure 1(c), the following holds true:*

(a) There exists a stable equilibrium at $(J^*, I^*) = (\gamma N, r/e)$.

(b) When the initial state $(J_0, I_0) = (J^*, I^*)$, then (J, I) remain constant while S, R take a linear form and β increases till the susceptible population reaches 0 at T_{end}.
(i) $S(t) = S_0 - \gamma I^* t;\ \ R(t) = R_0 + \gamma I^* t$
(ii) $\beta(t) = \frac{\gamma N}{S_0 - \gamma I^* t};\ \ T_{end} = \frac{S_0}{\gamma I^*}$

Proof of Theorem A.1 (a)
At equilibrium (J^*, I^*), we have $\dot{J} = 0$ and $\dot{I} = 0$. From the derivative of J in Section 2, it follows that

$$\dot{J}|_{(J,I)=(J^*,I^*)} = rJ^* - eI^*J^* = 0 \Rightarrow I^* = \frac{r}{e},$$
$$\dot{I}|_{(J,I)=(J^*,I^*)} = \frac{J^*I^*}{N} - \gamma I^* = 0 \Rightarrow J^* = \gamma N.$$

To prove the stability of the critical point at (J^*, I^*), let us consider the normalized variables $\phi(t) = \big(x(t), y(t)\big)$ where $x(t) = \frac{J(t)}{J^*}$ and $y(t) = \frac{I(t)}{I^*}$.
$\mathbf{z}^* = (1, 1)$ is the corresponding critical point.

$$||\phi(0) - \mathbf{z}^*||^2 = (x_0 - 1)^2 + (y_0 - 1)^2 < \delta^2$$
$$\Rightarrow 1 - \delta < x_0 < 1 + \delta,\ 1 - \delta < y_0 < 1 + \delta.$$

Let $f(s) = s - \log(s) - 1$. Since $f(s)$ is a convex function, $1 - \delta < s < 1 + \delta$, implies $f(s) < \max\{f(1+\delta), f(1-\delta)\}$. Denoting this bound by D_{max} implies $f(x_0) < D_{max}$ and $f(y_0) < D_{max}$
From Theorem 2(a), we note that

$$w(J_0, I_0) = \gamma f(x_0) + r f(y_0)$$
$$< (r + \gamma) D_{max}$$

[1] Theorem 1 is split into Theorem A.1 and Theorem A.2

Denoting $w_b = (r+\gamma)D_{max}$, from Theorem 2(a), we note that

$$w(J(t), I(t)) = w(J_0, I_0) < w_b$$
$$\Rightarrow f\big(x(t)\big) < \frac{w_b}{\gamma}, \;\; f\big(y(t)\big) < \frac{w_b}{r}.$$

Given the nature of $f(s)$, $f(s) < c \Rightarrow s_{min} < s < s_{max}$ where (s_{min}, s_{max}) are the finite-valued roots of $f(s) = c$. Hence $x(t)$ and $y(t)$ are both bounded on either side. Consequently, $(x(t)-1, y(t)-1)$ is confined to a bounded rectangle and thus,

$$\begin{aligned} \Rightarrow ||\phi\big(x(t), y(t)\big) - \mathbf{z}^*||^2 &= \big(x(t)-1\big)^2 \\ &\quad + \big(y(t)-1\big)^2 \\ &< \epsilon^2 \end{aligned}$$

where ϵ can be directly expressed in terms of δ and vice versa.
Hence, from Definition A.1, $\mathbf{z}^* = (1,1)$ (or equivalently (J^*, I^*)) is a stable equilibrium. ■

Proof of Theorem A.1 (b)

When initial state (J_0, I_0) is at equilibrium $(J^*, I^*) = (\gamma N, r/e)$, we have $(J(t), I(t)) = (\gamma N, r/e)$, $\forall t$. Hence,

$$\dot{S} = -\frac{\beta S I^*}{N} = -\frac{J^* I^*}{N} = -\gamma I^*$$
$$\Rightarrow S(t) = S_0 - \gamma I^* t.$$

Similarly,

$$\dot{R} = \gamma I^* \Rightarrow R(t) = R_0 + \gamma I^* t,$$
$$\beta(t) = \frac{J(t)}{S(t)} = \frac{\gamma N}{S_0 - \gamma I^* t}.$$

At $t = T_{end}$, the susceptible population $S(t) = 0$. Hence,

$$S(T_{end}) = 0 \Rightarrow T_{end} = \frac{S_0}{\gamma I^*}.$$

■

Theorem A.2 *For the LVSIR model in Figure 1(c), if the initial state is not at equilibrium, i.e., $(J_0, I_0) \neq (J^*, I^*)$, it exhibits a cyclic behaviour with the following properties.*

(a) The system "energy" $w(J, I) = \gamma(x - \log(x) - 1) + r(y - \log(y) - 1)$ (where $x = \frac{J}{J^*}, y = \frac{I}{I^*}$) remains constant at $w_0 = w(J_0, I_0) \geq w(J^*, I^*) = w^* = 0$ till termination.

(b) The I, J curves exhibit periodic oscillations resulting in a closed trajectory. The normalized phase plot has four extreme points $\{(x_{min}, 1), (1, y_{min}), (x_{max}, 1), (1, y_{max})\}$ where (x_{min}, x_{max}) are the roots of the equation $x - \log(x) = 1 + w_0/\gamma$ and (y_{min}, y_{max}) are the roots of the equation $y - \log(y) = 1 + w_0/r$.

(c) The cyclic period is given by

$$T_{period} = \int_{\log(x_{min})}^{\log(x_{max})} \left(\frac{1}{F_1^{-1}(G(z))} - \frac{1}{F_2^{-1}(G(z))}\right) dz,$$

where (x_{min}, x_{max}) are defined as above, $G(z) = \gamma(e^z - z - 1) - w_0$, and $F_1(s),\ F_2(s)$ are restrictions of $F(s) = s + r\log(1 - \frac{s}{r})$ to positive and negative ranges. In general, T_{period} has the form $g(r, \gamma, \frac{w_0}{r})$ with approximation via linearization yielding $T_{period} \simeq \frac{2\pi}{\sqrt{(r\gamma)}}$.

(d) In each cyclic period, S reduces by a fixed amount $\Delta S = \gamma I^* T_{period}$. When the susceptible population $S < \Delta S$ at the beginning of a cycle, it reaches 0 during the cycle and the epidemic terminates.

Proof of Theorem A.2 (a)
The energy function of the LVSIR system in Figure 2(c) corresponds to

$$w(J,I) = \gamma\left(\frac{J}{J^*} - \log\left(\frac{J}{J^*}\right) - 1\right) + r\left(\frac{I}{I^*} - \log\left(\frac{I}{I^*}\right) - 1\right),$$

and the dynamics of I, J are given by

$$\dot{J} = (r - eI)J = r\left(1 - \frac{I}{I^*}\right)J$$

$$\dot{I} = \left(\frac{J}{N} - \gamma\right)I = \gamma\left(\frac{J}{J^*} - 1\right)I.$$

Considering the time derivative of $w(J,I)$, we have

$$\begin{aligned}
\dot{w}(J,I) &= \gamma\left(\frac{\dot{J}}{J^*} - \frac{\dot{J}}{J}\right) + r\left(\frac{\dot{I}}{I^*} - \frac{\dot{I}}{I}\right) \\
&= \gamma\dot{J}\left(\frac{1}{J^*} - \frac{1}{J}\right) + r\dot{I}\left(\frac{1}{I^*} - \frac{1}{I}\right) \\
&= \gamma r J\left(1 - \frac{I}{I^*}\right)\left(\frac{1}{J^*} - \frac{1}{J}\right) \\
&\quad + r\gamma I\left(\frac{J}{J^*} - 1\right)\left(\frac{1}{I^*} - \frac{1}{I}\right) \\
&\text{(substituting for } \dot{I},\ \dot{J}) \\
&= r\gamma\frac{(I^* - I)(J - J^*)}{I^*J^*} \\
&\quad + r\gamma\frac{(I - I^*)(J - J^*)}{I^*J^*} \\
&= 0
\end{aligned}$$

Hence, $w(J,I)$ remains invariant throughout and is equal to $w(J_0, I_0) = w_0$. ■

Proof of Theorem A.2 (b)
Let $w_0 = w(J_0, I_0)$ be the energy associated with the modified SIR system in Figure 2(c). The conservation law implies that every valid state (J,I) corresponds to a point on the level curve given by

$$\begin{aligned}
w(J,I) &= \gamma\left(\frac{J}{J^*} - \log\left(\frac{J}{J^*}\right) - 1\right) \\
&\quad + r\left(\frac{I}{I^*} - \log\left(\frac{I}{I^*}\right) - 1\right) \\
&= w_0
\end{aligned}$$

If J, I functions are continuous[2], then these would be periodic functions. In terms of normalized variables, $x = \frac{J}{J^*}$ and $y = \frac{I}{I^*}$, the phase plot reduces to

$$\gamma(x - \log(x) - 1) + r(y - \log(y) - 1) = w_0.$$

Consider the continuously differentiable function $f(z) = z - \log(z) - 1$ defined on $\mathbb{R}_{++}$. Since $\frac{df}{dz} = 1 - \frac{1}{z}$ and $\frac{d^2f}{dz^2} = \frac{1}{z^2} > 0$, $f(z)$ is a convex function with a single global minimum at $z = 1$ corresponding to $f(1) = 0$. Hence $f(z) \leq c \Rightarrow z_{min} \leq z \leq z_{max}$ where (z_{min}, z_{max}) correspond to the roots of $f(z) = c$.

[2]Note that J, I are actually discrete population counts and not continuous functions.

To identify the extreme x values, we observe that

$$\begin{aligned} \gamma(x - \log(x) - 1) + r(y - \log(y) - 1) &= w_0 \\ \Rightarrow \gamma(x - \log(x) - 1) &\leq w_0 \\ (\text{ since } f(y) > 0) & \\ \Rightarrow x_{min} \leq x \leq x_{max} & \end{aligned}$$

where (x_{min}, x_{max}) are roots of $f(x) = \frac{w_0}{\gamma}$. Both the extreme values of x are realized for $y = 1$. Similarly, the extreme values of y are attained for $x = 1$ and given by (y_{min}, y_{max}) which correspond to the roots of $f(x) = \frac{w_0}{r}$.

■

Proof of Theorem A.2 (c)
The period of a Lotka-Volterra system has been derived in multiple works Shih (1997). We include the below proof based on Hsu's method Hsu (1983) for completeness.

Let $x = \frac{J}{J^*}$ and $y = \frac{I}{I^*}$. Then we have

$$\dot{x} = -rx(y - 1) \tag{1}$$

$$\dot{y} = \gamma y(x - 1). \tag{2}$$

From 1, we have

$$\begin{aligned} \ddot{x} &= -rx\dot{y} - r\dot{x}(y - 1) \\ &= -rx\gamma y(x - 1) - r(y - 1)\dot{x} && \text{(substituting } \dot{y} \text{ from 2)} \\ &= -r\gamma x(-\frac{\dot{x}}{rx} + 1)(x - 1) + \frac{r(\dot{x})^2}{rx} && \text{(substituting y from 1)} \\ &= -\gamma(rx - \dot{x})(x - 1) + \frac{\dot{x}^2}{x} \end{aligned}$$

Thus,

$$\ddot{x} - \frac{\dot{x}^2}{x} - \gamma(x - 1)(\dot{x} - rx) = 0. \tag{3}$$

Let $z = \log(x)$. Then, $\dot{x} = e^z\dot{z}$ and $\ddot{x} = e^z(\ddot{z} + \dot{z}^2)$.

From 3, we have

$$\begin{aligned} e^z(\ddot{z} + \dot{z}^2) - \frac{e^{2z}(\dot{z})^2}{e^z} & \\ -\gamma(e^z - 1)(e^z\dot{z} - re^z) &= 0 \\ \Rightarrow \ddot{z} - \gamma(e^z - 1)(\dot{z} - r) &= 0. \end{aligned}$$

Choosing $s = \dot{z} \Rightarrow s = \frac{\dot{x}}{x} = -r(y - 1)$.

Let $w_0 = w(J_0, I_0)$. Then, the trajectory corresponds to

$$\begin{aligned} & \gamma(x - \log x - 1) + r(y - \log y - 1) = w_0 \\ \Rightarrow\ & \gamma(e^z - z - 1) + r(y - \log y - 1) = w_0 \\ \Rightarrow\ & \gamma(e^z - z - 1) + r(-\frac{s}{r} - \log(1 - \frac{s}{r})) = w_0 \\ \Rightarrow\ & \gamma(e^z - z - 1) - w_0 = s + r\log(1 - \frac{s}{r}) \\ \Rightarrow\ & G(z) = F(s) \end{aligned}$$

where $G(z) = \gamma(e^z - z - 1) - w_0$ and $F(s) = s + r\log(1 - \frac{s}{r})$.

Let $F_1(s), F_2(s)$ be the restrictions of $F(s)$ for the lower and upper parts of the phase plot. Then the time period for the lower section is given by

$$\int_{z_{min}}^{z_{max}} \frac{dz}{s} = \int_{z_{min}}^{z_{max}} \frac{dz}{F_1^{-1}(G(z))}.$$

The total time for both the lower and upper section is given by

$$\int_{\log(x_{min})}^{\log(x_{max})} \left(\frac{1}{F_1^{-1}(G(z))} - \frac{1}{F_2^{-1}(G(z))} \right) dz.$$

When $w_0 \simeq 0$, linearization is possible. Simplifying the trajectory $F(s) = G(z)$ using the approximations $e^a = 1 + a + \frac{a^2}{2}$ and $\log(1 - a) = a - \frac{a^2}{2}$, we have

$$\begin{aligned}
&\gamma(e^z - z - 1) - w_0 = s + r\log(1 - \frac{s}{r}) \\
&\Rightarrow \frac{\gamma z^2}{2} - w_0 = s + r(-\frac{s}{r} - \frac{s^2}{2r^2}) \\
&\Rightarrow \frac{\gamma z^2}{2} + \frac{s^2}{2r} = w_0
\end{aligned}$$

Essentially, we have an elliptical curve with x, y following sinusoidal behavior with a period $\frac{2\pi}{\sqrt{r\gamma}}$. ■

Proof of Theorem A.2 (d)
Assuming a continuous form for J, we observe that

$$\begin{aligned}
\dot{J} &= (r - eI)J \\
\Rightarrow \frac{1}{J}\frac{dJ}{dt} &= r - eI \\
\frac{d}{dt}(\log(J)) &= r - eI \\
\int_{t=t_0}^{t=t_0+T_{period}} d(\log(J)) &= \int_{t=t_0}^{t=t_0+T_{period}} (r - eI)dt \\
&\text{(since } J \text{ is periodic)} \\
\int_{t=t_0}^{t=t_0+T_{period}} d(\log(J)) &= 0 \text{ (for any } t_0) \\
\Rightarrow \int_{t=t_0}^{t=t_0+T_{period}} Idt &= \frac{r}{e}T_{period} \\
&= I^* T_{period}
\end{aligned}$$

In other words, I^* is also the average value of I in each cycle.

Considering the time derivatives of S and I, we have $\dot{I} = \frac{\beta SI}{N} + \gamma I$ and $\dot{S} = -\frac{\beta SI}{N}$.

Let ΔS be the drop in S during a single cycle starting at any t_0, then

$$\begin{aligned}
\Delta S &= \int_{t=t_0}^{t=t_0+T_{period}} \dot{S} dt \\
&= \int_{t=t_0}^{t=t_0+T_{period}} (-\dot{I} + \gamma I) dt \\
&\quad \text{(since } \dot{I} = -\dot{S} + \gamma I\text{)} \\
&= 0 + \gamma \int_{t=t_0}^{t=t_0+T_{period}} I dt \\
&\quad \text{(since } I \text{ is periodic)} \\
&= \gamma I^* T_{period} \text{ (from above)}
\end{aligned}$$

■

B Optimal Transmission Rate Control (CoSIR)

Definition B.1 *Given a dynamical system $\dot{\mathbf{z}} = \mathbf{f}(\mathbf{z}, \mathbf{u})$ with state vector $\mathbf{z} \in D \subset \mathbb{R}^{\mathrm{n}}$, control $\mathbf{u} \in \mathbb{R}^{\mathrm{m}}$, and equilibrium state $\mathbf{z}^* = \mathbf{0}$, a control-Lyapunov function (CLF) is a function $V : D \mapsto \mathbb{R}$ that is continuously differentiable, positive-definite s.t. $\forall \mathbf{z} \neq 0, \exists\, \mathbf{u}$, $\dot{V}(\mathbf{z}, \mathbf{u}) = \langle \nabla V(\mathbf{z}), \dot{\mathbf{z}} \rangle = \langle \nabla V(\mathbf{z}), \mathbf{f}(\mathbf{z}, \mathbf{u}) \rangle < 0$.*

The CLF $V(\cdot)$ can be viewed as a generalized energy function with $\dot{V}(\cdot)$ being a dissipation function. Artstein (1983) proved that as long as there is a CLF, there exists a control $\mathbf{u}$ to ensure the reduction of energy at every non-equilibrium state and eventual convergence to the zero energy equilibrium.

Theorem B.1 (Artstein (1983)) *For any non-linear dynamical system with affine control, $\dot{\mathbf{z}} = \mathbf{f}(\mathbf{z}, \mathbf{u}) = \mathbf{f_0}(\mathbf{z}) + \sum_{i=1}^{m} \mathbf{f_i}(\mathbf{z}) u_i$ with state $\mathbf{z} \in D \subset \mathbb{R}^{\mathrm{n}}$, control $\mathbf{u} \in \mathbb{R}^{\mathrm{m}}$, has a CLF if and only if it admits a regular stabilizing control feedback $\mathbf{u}$, that is a locally Lipschitz function on $\mathbb{R}^{\mathrm{n}} \setminus \{0\}$.*

Once a CLF is identified, it is relatively straightforward to design an appropriate control function $\mathbf{u}$ as described in (Artstein, 1983; Tsinias, 1989). For our scenario, we rely on the conservation law of the LV system as well as the existing literature on its Lyapunov functions (Pykh, 2001).

We follow a similar approach to construct CLFs from the "Lotka-Volterra energy" function $w(J, I)$. Let $\mathbf{z} = (\frac{J}{J^*} - 1, \frac{I}{I^*} - 1)$ so that the equilibrium $\mathbf{z}^* = (0, 0)$. Let $L(w) : \mathbb{R}_+ \mapsto \mathbb{R}$ be a continuously differentiable function s.t. $|dL/dw| > 0$ and $L(w) > 0$, $\forall w$ and $L(w) = 0 \iff w = 0$. The function $L(w(J, I))$ can be used as a CLF for the SIR model. Examples include L_p norms and Bregman divergences. Using this CLF, we design an optimal control policy for SIR.

Theorem B.2 (CoSIR) *For the SIR model, a proportional additive control on β of the form,*

$$\dot{\beta} = (r - eI)\beta + \frac{\beta^2 I}{N} + u\beta \tag{4}$$

converges to the equilibrium (J^*, I^*) when

$$u = -\eta(t) \frac{dL}{dw} \left(\frac{J}{J^*} - 1 \right)$$

with the learning rate $\eta(t) > 0$, $\forall t$.

Proof of Theorem B.2
Assuming a proportional additive control on β of the form $\dot{\beta} = \frac{\beta^2 SI}{N} + (r - eI)\beta + u\beta$, the variation

of the susceptible contacts J is given by

$$\begin{aligned}\dot{J} &= \dot{\beta}S + \beta\dot{S} \\ &= \left(\frac{\beta^2 SI}{N} + (r - eI)\beta + u\beta\right) S \\ &\quad + \beta\left(-\frac{\beta SI}{N}\right) \\ &= (r - eI + u)J\end{aligned}$$

Let $\mathbf{z} = (J/J^* - 1, I/I^* - 1) = (z_1, z_2)$ so that $\mathbf{z} = (0, 0)$ corresponds to the equilibrium state. Then $w(J, I) = \gamma(z_1 - \log(1 + z_1)) + r(z_2 - \log(1 + z_2))$. For $V(\mathbf{z}) = L(w(J, I))$ to be a control-Lyapunov function, we require $\dot{V}(\mathbf{z}, \mathbf{u}) < 0$.

$$\begin{aligned}\dot{V}(\mathbf{z}, \mathbf{u}) &= \langle \nabla V(\mathbf{z}), \dot{\mathbf{z}} \rangle \\ &= \frac{dL}{dw}\langle \nabla w(\mathbf{z}), \dot{\mathbf{z}} \rangle \\ &= \frac{dL}{dw}\left(\frac{dw}{dz_1}\dot{z}_1 + \frac{dw}{dz_2}\dot{z}_2\right) \\ &= \frac{dL}{dw}\left(\gamma\Big(1 - \frac{1}{z_1 + 1}\Big)\dot{z}_1\right. \\ &\quad \left. + r\Big(1 - \frac{1}{z_2 + 1}\Big)\dot{z}_2\right) \\ &= \frac{dL}{dw}\left(\gamma\Big(\frac{J}{J^*} - 1\Big)u\right).\end{aligned}$$

When the control is chosen as

$$u = -\eta(t)\frac{dL}{dw}(\frac{J}{J^*} - 1)$$

and $\eta(t) > 0,\ \forall t$,

$$\begin{aligned}\dot{V}(\mathbf{z}, \mathbf{u}) &= \frac{dL}{dw}\left(\gamma\Big(\frac{J}{J^*} - 1\Big)\right) \\ &\quad \times \left(-\eta(t)\frac{dL}{dw}\Big(\frac{J}{J^*} - 1\Big)\right) \\ &= -\eta(t)\gamma\left(\frac{dL}{dw}\Big(\frac{J}{J^*} - 1\Big)\right)^2 \\ &< 0 \ \ (\text{unless } w = w^*)\end{aligned}$$

Hence, Artstein's theorem guarantees convergence to the equilibrium. ∎

C PARAMETER CHOICES

Table 3 enumerates the detailed parameter choices and the relevant assumptions. In case of parameters that vary across regions (e.g., hospitalization rate, infection fatality rate), we have attempted to use estimates listed in existing literature. However, there are often variations across multiple studies and we chose a single reasonable value. Note that the key insights on the relative behavior of the transmission control policies hold true regardless of the specific choices of the parameter values.

Factor	Notation	Hypothetical	India
Population	N	13M	1.366B
Stage of pandemic	(S_{curr}, I_{curr})	(12.6M, 0.2M)	(1.36B, 279k)
Bed Occupancy level (Phillip et al., 1984)	κ	-	0.76
Medical Capacity (per capita) (OECD, 2020)	p	-	5.3×10^{-4}
Hospitalization ratio	h	-	2%
Time spent in hospital	T_{hosp}	-	20 days
Target manageable hospitalizations	ΔH_{avg}^{target}	-	27.5k
Target manageable infections	I_{avg}^{target}	0.15M	6.88M
Target max to average ratio	$I_{max}^{target}/I_{avg}^{target}$	1.3	1.13
Infection-Fatality ratio (Meyerowitz-Katz & Merone, 2020; Mukhopadhyay & Chakraborty, 2020; Murhekar et al., 2020)	IFR	-	0.002 [3]
Death detection ratio	DDR	-	0.3
Reported Infections on 1st Dec 2020 (COVID19India, 2020)		-	9.5M
Reported Fatalities on 15th Dec 2020 (COVID19India, 2020)		-	144k
Under reporting factor	URF	-	25.28
Periodicity	T_{period}	7 days	7 days
Reciprocal of infectious period	γ	0.2	0.2
LV Reproduction rate	r	4.2	4.2
Consumption rate	e	2.8×10^{-5}	6.1×10^{-7}
Initial transmission rate	β_0	0.2	0.2
Learning rate	η	5	5

Table 3: State of the epidemic, public health requirements, and CoSIR parameters used for the simulations in Section 3.

The various parameters can be broadly divided into three groups discussed below.

(a) Target Hospitalization & Infectious levels. There are multiple ways to arrive at an acceptable level for infectious population I_{avg}^{target} based on socioeconomic impact considerations (BMGF, 2020). When the focus is on medical capacity constraints, this target level can be set chosen so that the available medical capacity can meet the hospitalization requirements at a steady state. Let p denote the per-capita hospital bed capacity of a region with population N, κ the bed occupancy level for normal functioning, and T_{hosp} the average duration of hospitalization. Then, a manageable hospitalization inflow that will not overwhelm the medical infrastructure is given by $\Delta H_{avg}^{target} = \frac{Np\kappa}{T_{hosp}}$. As described earlier in Section 3, assuming SIR dynamics, the new hospitalizations would be given by $\gamma h I$. Hence, we choose the target infectious level as $I_{avg}^{target} = \frac{Np\kappa}{\gamma h T_{hosp}}$. To concretely instantiate these choices for various regions, we use the populations of the regions N, the per-capita medical capacity (OECD, 2020) assuming an average hospitalization period $T_{hosp} = 20$ days and hospitalization ratio 2%.

(b) Under Reporting Factor. While comparing real observed case counts with simulations, a critical factor to consider is the level of under reporting. This factor was computed based on the assumption that the infection fatality rate (IFR) and death detection rate (DDR) are largely variant within a region and there is a steady lag of 2 weeks between infection and the associated fatalities. In particular, we estimate the under reporting factor (URF) as

$$\begin{aligned} URF &= \frac{\text{Reported Infections}}{\text{Total Infections}} \\ &= \frac{(\text{Reported Infections on Dec 1st}) \times DDR \times IFR}{\text{Reported Fatalities on Dec 15th}} \end{aligned}$$

The purpose of computing URF is to figure out the appropriate scaling of real cases for a fair comparison with the simulated results.

(c) SIR & CoSIR Parameters. The primary parameter of interest in the SIR model apart from the transmission rate is γ, i.e., reciprocal of the infectious period, which was chosen to be 0.2 across all simulations since it is a disease-specific factor. For practical implementation of a control policy, a periodicity aligned with typical economic activity is preferable and hence, we choose $T_{period} = 7$ days for the CoSIR variants. Assuming the maximum value of infections to be 13% higher than the average and following Algorithm 1, we obtain the LV reproductive rate $r = 4.2$. We choose the

steady state infectious level to be the target infectious level, i.e., $I^* = I_{avg}^{target}$ and the consumption rate is given by $e = r/I^*$. To ensure effective control, we pick an aggressive learning rate $\eta = 5$.

D RESTRICTION LEVELS AND TRANSMISSION RATES

Restriction level	**Effective R value**	**COVID-19 Transmission rate (β)**	**Description**
Early event (Pre-restrictions)	2.52	0.4	No policy interventions.
Lockdown	0.84	0.12	Residents are either not allowed to leave their residence or may leave only for essential functions.
Stay-at-home	0.95	0.14	Stay-at-home order includes closure of schools and private sector, and restrictions on mass gatherings.
Safer-at-home	1.26	0.19	Relaxed stay-at-home order which includes closure of schools, but restrictions on mass gatherings and private sector may be relaxed.
New normal	1.83	0.29	Stay-at-home lifted or relaxed with some restrictions on mass gatherings and private sector. Schools may or may not be re-opened. Safeguards such as face coverings encouraged.

Table 4: Example of restriction levels recommended by public health authorities (COVID-AMP, 2020) and the corresponding effective R value and transmission rate (β) for COVID-19.

E LARGE FIGURES

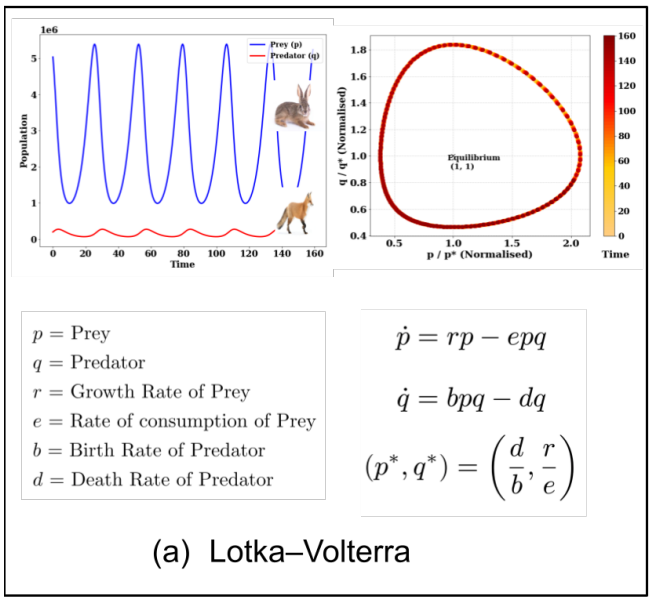

Figure 4: (a) Lotka-Volterra system and evolution of predator (fox) and prey (hare) population over time.

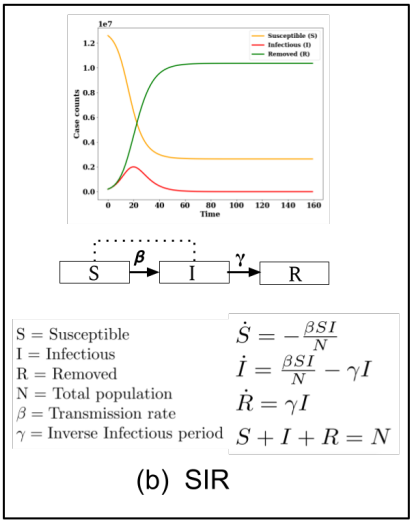

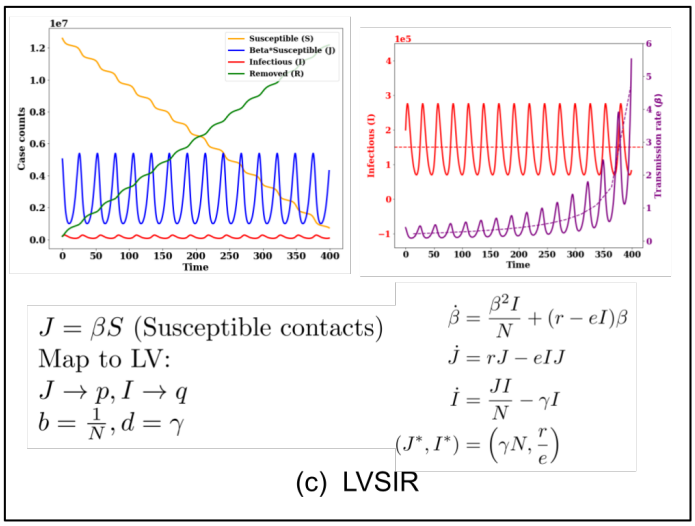

Figure 5: (b) SIR compartmental dynamics for epidemiological modeling. (c) Mapping of SIR model to LV system and the behaviour of case counts S, J, I, R and transmission rate β.

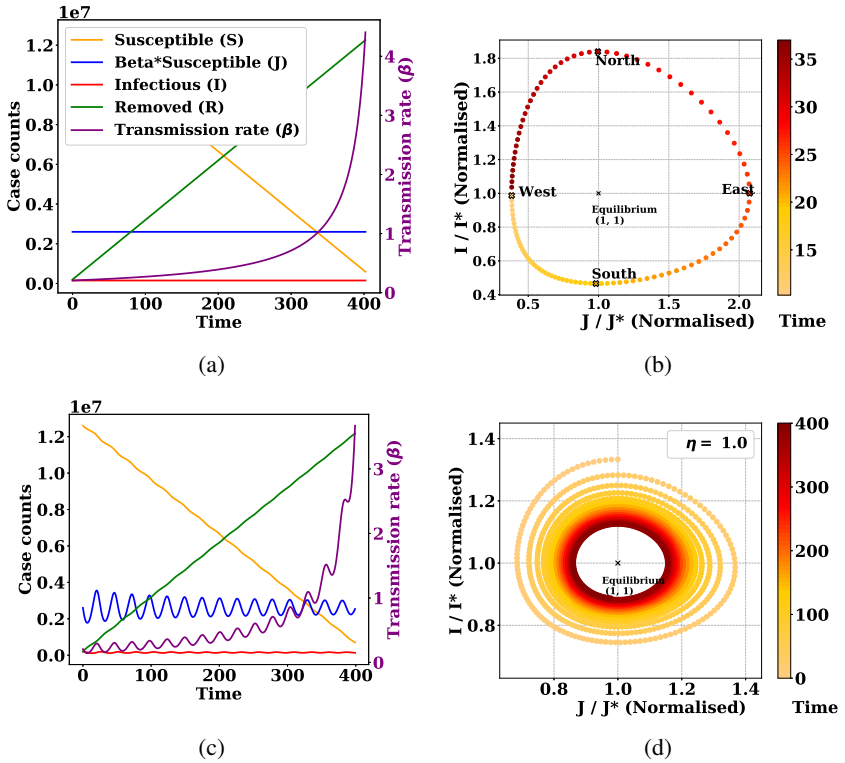

Figure 6: (a) System (S, J, I, R, β) evolution when initialized at equilibrium. (b) Phase plot of the LVSIR model annotated with extreme points. (c-d) System evolution of the CoSIR model for learning rate $\eta = 1$.

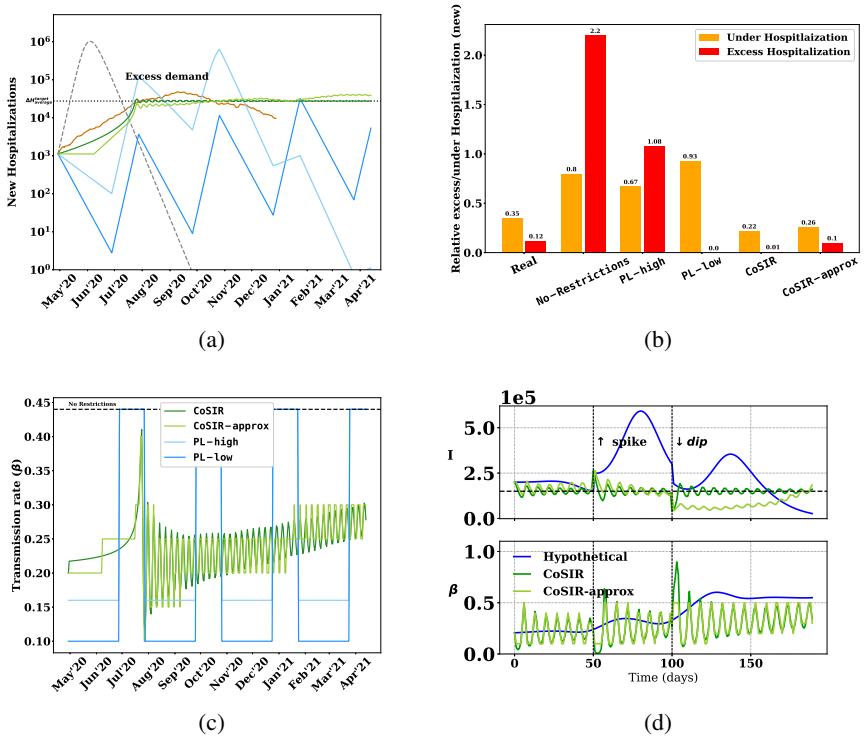

Figure 7: Plots (a-c) show the hospitalization inflow, its comparison to ΔH_{avg}^{target} and $\beta(t)$ for various policies in India. (d) Shows the adaptive nature of CoSIR variants to a sudden increase or decrease ($t = 50, 100$).